MRS Advances (2022) 7:383–387
https://doi.org/10.1557/s43580-022-00237-y

ORIGINAL PAPER

Hydrogen adsorption in phase and grain boundaries of pearlitic steels and its effects on tensile strength

Xiaoli Wang[1] · Yonghao Zhao[1] · Guang Cheng[1] · Yang Zhang[1] · T. A. Venkatesh[2]

Received: 2 January 2022 / Accepted: 9 February 2022 / Published online: 22 February 2022

Abstract

Molecular dynamic simulations are invoked to study hydrogen (H) adsorption as well as its effects on the strength of pearlitic steels. In particular, the effects of H on the strength of the cementite (Fe_3C)–ferrite interphase and the ferrite–ferrite grain boundaries are investigated. It is observed that the thickness of the cementite phase and the ferrite grain boundary orientation influences H adsorption: the amount of adsorbed H atoms decreases linearly with the thickness of the cementite phase; the Σ3 ferrite grain boundaries with ~ 30° or 75° orientation trap the most H atoms. Upon comparing the tensile strength of atomic structures before and after the H adsorption, it is observed that the strength of the cementite–ferrite interface is increased after H adsorption. H adsorption and H cluster formation at or near the grain boundaries are observed to affect the strength and failure modes of the ferrite–ferrite grain boundaries.

Introduction

The influence of hydrogen on the mechanical properties of materials has been extensively studied. Three mechanisms, i.e., hydrogen-enhanced decohesion [1, 2], hydrogen-enhanced localized plasticity [3, 4], and hydrogen-enhanced strain-induced vacancy formation [5, 6], have been proposed to explain the brittle intergranular fracture observed in ferritic steels, enhanced dislocation mobility observed in Ni and Ni–C alloys, and the reduced mobility of H atoms due to trapping by vacancies, respectively. Some aspects of the mechanisms that contribute to H-induced damage have been validated by experiments.

While the effects of hydrogen on the material's behavior can be readily characterized at the macroscale level, it is still challenging to directly observe the H adsorption process at the microstructural level. Hence, the precise nature of the interactions between H and microstructural features, such as internal defects, secondary phase particles, grain boundaries, as well as H's effects on mechanical deformation, have not been fully understood.

With the development of potential functions for the interactions between H, Fe, C, and other elements within steels [7] over the past decade, molecular dynamics simulations have been used to investigate H adsorption and H interactions with internal defects of steels, such as vacancies and dislocations. The effect of H on dislocation mobility in α-ferrite lattice has been analyzed using nano-scale simulation [3, 4, 8]. The effect of H on the mobility of the grain boundaries has also been explored [9–11], and improved strength of the H-adsorbed material, attributed to the obstacle effect of H atoms, has been reported as well.

Recently, advances in atom probe tomography have enabled a detailed characterization of the actual distribution of H atoms in a H-charged ferritic steel [11, 12]. It is believed that the interfaces within the microstructure, such as the carbide–ferrite interface and the ferrite–ferrite grain boundaries, are more likely to trap the H atoms. Therefore, these phase boundaries and grain boundaries are expected to play critical roles in designing steels that resist H-induced damage. Hence, the present study is focused on understanding H adsorption at two types of internal interfaces: the ferrite–cementite phase boundary and the ferrite–ferrite grain boundary. Since most grain boundaries within the microstructure are asymmetric [13, 14], the asymmetric tilt grain

T. A. Venkatesh was an editor of this journal during the review and decision stage. For the MRS Advances policy on review and publication of manuscripts authored by editors, please refer to mrs.org/editor-manuscripts.

✉ Guang Cheng
guangcheng@mail.buct.edu.cn

[1] College of Mechanical and Electrical Engineering, Beijing University of Chemical Technology, Beijing 100029, China

[2] Department of Materials Science and Chemical Engineering, Stony Brook University, Stony Brook, NY 11794, USA

boundaries are chosen for this study. Molecular dynamics simulations are invoked to analyze the effects of cementite thickness and the ferrite–ferrite grain boundary orientation on H adsorption at the phase boundaries and grain boundaries and to assess the strength of these interfaces.

Modeling setup

The atomic structures were generated in the visualization and analysis software, OVITO [15], and all the molecular dynamics simulations were conducted in LAMMPS [16]. There are three essential elements: Fe, C, and H, in pearlitic steels. Correspondingly, three pairwise potential functions were adopted in the current study: (i) the modified embedded atom method (MEAM) potential functions from Liyanage [17] were used for cementite (Fe_3C) since these functions have been validated by the experimentally obtained elastic modulus and thermal properties; (ii) the potential functions from Ramasuramaniam [7], which have been widely implemented in previous simulations [8–10], were utilized for the Fe–H interaction; and (iii) the MEAM potential functions from Nouranian [18] were used for the C–H interaction. Because two types of MEAM potential functions were utilized, additional computing capability was required to obtain the angular forces in the simulated systems. The number of atoms in the simulation model was about 300,000, and the time step was fixed at 0.1 fs.

As shown in Fig. 1a, the microstructures of pearlitic steels that were modeled exhibited two characteristic interfaces—phase boundaries and grain boundaries. Eight models of ferrite–cementite interfaces with different thicknesses of the cementite phase, as shown in Fig. 1b, were developed. Since the ferrite–cementite interfaces should satisfy the orientation relationship proposed by Bagaryatsky [19], the *X*, *Y*, and *Z* directions were selected to conform to the combination of ferrite/cementite directions as $[111]_{ferrite}//[010]_{cementite}$, $(112)_{ferrite}//(010)_{cementite}$, and $[1\bar{1}0]_{ferrite}//[100]_{cementite}$, respectively. The interface was along the *X*–*Z* plane. The thickness of the cementite in the diffusion simulation varied from 1.4 to 11.4 nm. Of the eight structures considered, four, denoted as C-1, C-2, C-3, and C-4, with cementite thickness of 1.4 nm, 2.8 nm, 5.7 nm, and 11.4 nm, respectively, were analyzed for the effects of H adsorption on the interfacial strength. The model size was 11.5 nm in the *X*-direction, 25.8 nm in the *Y*-direction, and 11.5 nm in the *Z*-direction.

Furthermore, Σ3 grain boundaries were constructed to study H adsorption at the asymmetric ferrite tilt grain boundary. Using the *X*-axis as the rotation axis, two adjacent ferrite grains were rotated to different degrees (φ: 10.02°, 29.50°, 64.76°, and 81.95°) in ATOMSK [20]. The total angle (θ) was kept at 109.47°, as shown in Fig. 1c. Grain boundaries with eight angles were implemented in the H diffusion simulation, and four of them (named as GB-1, $\varphi = 10.02°$; GB-2, $\varphi = 29.50°$; GB-3, $\varphi = 64.76°$; GB-4, $\varphi = 81.95°$) were selected for detailed analysis.

In the H adsorption simulation, about 0.08% H atoms were randomly distributed in the ferrite grains within the model structure to mimic long-time H diffusion or charging. The initial temperature was set to 300 K, and periodic boundary conditions were applied in the three directions. The conjugate gradient algorithm was utilized to optimize the initial system. The H diffusion and adsorption process were allowed to take place over 100 ps in the isothermal–isobaric condition to ensure saturation in H adsorption. The damping parameters for isothermal–isobaric ensemble are temperature damping parameter (T_{damp}) = 100 timesteps and pressure damping parameter (P_{damp}) = 1000 timesteps, respectively. The tensile test simulations were conducted in the isothermal–isobaric condition with a 10^9/s strain rate. The limitations of

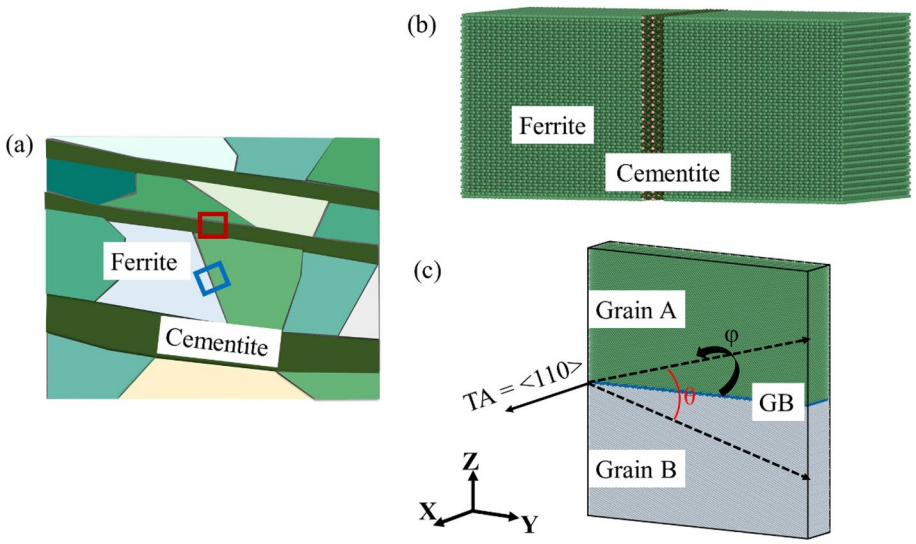

Fig. 1 **a** The illustration of the microstructure with grain boundaries and phase boundaries, **b** the ferrite–cementite interfacial structure as the red box highlighted in figure **a**, and **c** the sketch of atomic structure with grain boundaries as the blue box highlighted in figure **a**

Molecular dynamic (MD) simulations usually permit simulations of tensile tests at high strain rates. There is a possibility that some deformation mechanisms that are dominant at lower strain rates and observed in experiments conducted at lower strain rates may not be captured in the MD simulations. Thus, a direct comparison of MD simulation results to experiments is possible if the experiments are also conducted at equivalent high strain rates. However, within the limits of MD simulations, this study aims to obtain trends in the mechanical response of the material to H adsorption at the phase boundary and grain boundary interfaces.

Results and discussion

Hydrogen adsorption at the phase boundaries (ferrite–cementite interfaces)

Since the H atoms were mainly adsorbed by the carbon atoms in the cementite, the H atoms were considered to be adsorbed if the distance between one H atom and one C atom was less than 0.15 nm, which is the length of the C–C covalent bond. An in-house code was developed to record the atomic positions and obtain the number of captured H atoms. Then, the number of H atoms that was adsorbed at the interface, over time, was determined (Fig. 2a). It was observed that the initial adsorption rate was different in the four model structures considered. The structure with the thinnest cementite layer, C-1, had the highest H adsorption rate and took the longest time (~ 40 ps) to reach the saturation state with the most adsorbed H atoms. While the structure with the thickest cementite layer, C-4, had the lowest adsorption rate and reached the H saturation limit faster than other structures. The relationship between the cementite phase thickness and the total number of adsorbed H atoms was determined (Fig. 2b) as follows:

$$\text{The number of adsorbed H atoms} = 238.71 - 19.07t^2 + 0.63t^2 - 0.007t^3,$$

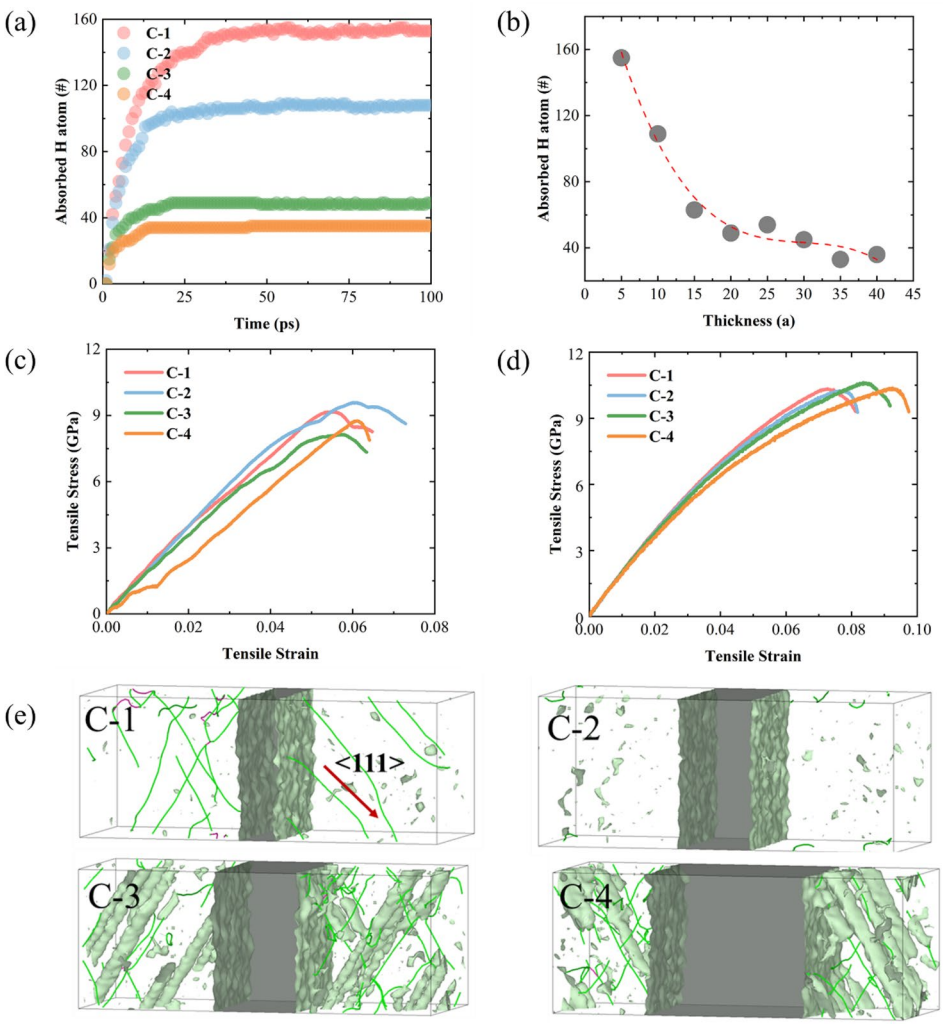

Fig. 2 **a** The absorbed H atoms number versus time for the four structures (from C-1 to C-4), **b** the absorbed H atoms and cementite thickness (a is the lattice parameter of α-Fe, and equal to 0.28 nm) with the fitted curve in red dash line, **c** the stress–strain curves of four structures before H adsorption, **d** the stress–strain curves of four structures after H adsorption, and **e** dislocation analysis of four structures at 10% strain

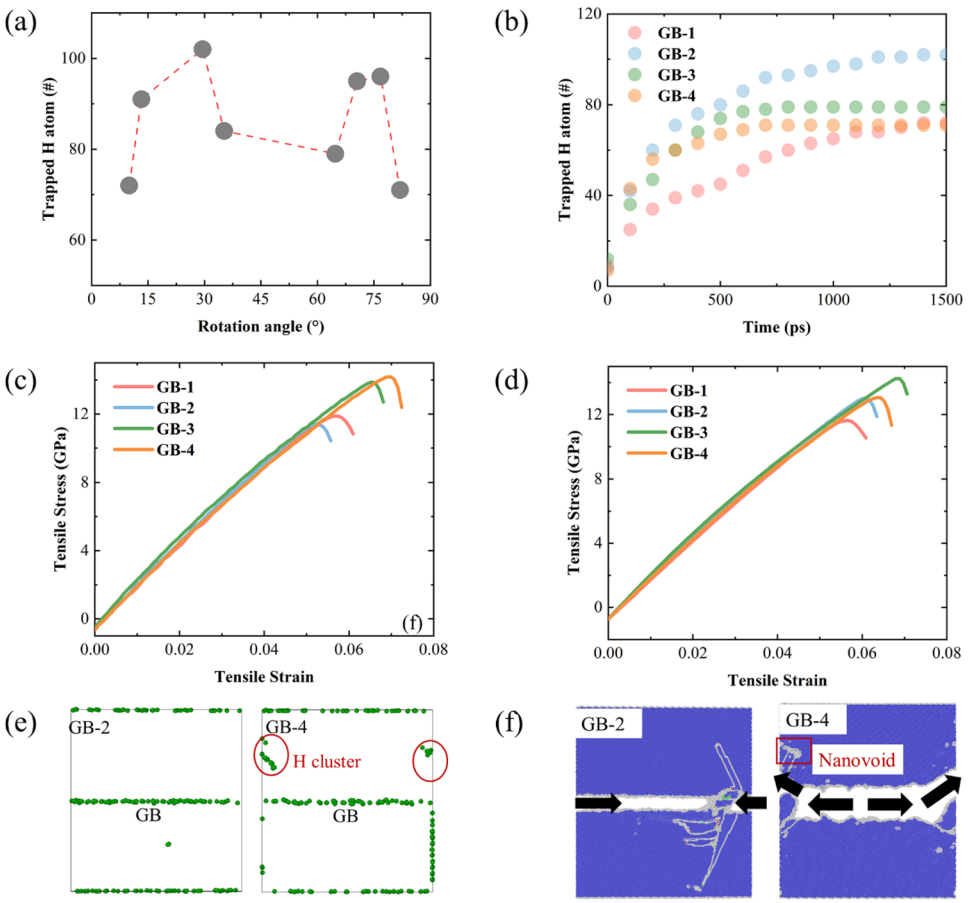

Fig. 3 **a** The absorbed H atoms with grain boundary rotation angles from 10.02° to 81.95°, **b** the number of absorbed H atoms versus time for the four structures with different grain boundary rotation angles, **c** the stress–strain curves of the four structures before H adsorption, **d** the stress–strain curves of the four structures after H adsorption, **e** H distribution within four structure after H diffusion with H clusters marked in red circles, and **f** common neighbor analysis of GB-2 and GB-4 structures

where t is the thickness of the cementite phase.

Subsequently, tensile stress was applied along the Y-direction on the four structures before and after the H adsorption. As shown in Fig. 2c and d, the strength of the ferrite–cementite interface was increased for all four structures after H adsorption. As observed in the response of the C-1 structure, the adsorption of more H atoms was correlated to a greater increase in the interfacial strength. In all the four structures that were analyzed, a certain level of dislocation activity was observed. Dislocations were generated near the ferrite–cementite interface and moved to the interior of the ferrite. However, comparatively more dislocations were generated and significant dislocation movements were observed in the H-adsorbed C-3 or C-4 structures, unlike in the case of C-1 or C-2 structures where the dislocation activity was much less. Thus, it can be reasoned that H adsorption decreases dislocation activity, reduces plastic deformation, and enhances the strength of the ferrite–cementite interface.

Hydrogen adsorption at the asymmetric tilt grain boundaries (ferrite–ferrite interfaces)

The thickness of the ferrite–ferrite grain boundary was about 1 nm after relaxation. The criterion for the H capture at the grain boundary was set as 0.5 nm distance from the grain boundaries. The models with grain boundary structures took much longer times (about 1200 ps) than the ferrite–cementite structures to reach H saturation. The four models (GB-1, GB-2, GB-3, and GB-4) showed different H adsorption behaviors within 1200 ps. The structure GB-2 adsorbed the most H atoms, and structure GB-1 or GB-4 adsorbed the fewest H atoms.

The strength of the ferrite–ferrite grain boundaries before and after H adsorption was compared, by applying a tensile stress and the resulting stress–strain responses of all the four structures are presented in Fig. 3c and d. The tensile strength of the structures GB-1 and GB-4 was reduced after H adsorption at the grain boundaries, especially for the GB-4 structure, where an 8.6% reduction was observed. On the contrary, the tensile strength of structures GB-2 and GB-3 was increased. A 12.5% increment was observed in the tensile strength of GB-2. While the precise mechanism that causes the strength of a grain boundary interface to increase or decrease with H is not clear, the differences in the stress field gradients near the grain boundary region (which arises due to the differences in the grain orientations) that influence H diffusion and the formation of H clusters during the diffusion process (as shown in Fig. 3e), which contributes to

the formation of nano-voids, could be important factors to be considered. As shown in Fig. 3f, failure of the grain boundary interface is initiated with the formation of a crack near the grain boundary in the GB-2/GB-4 structure. The crack then propagates along the interface and moves into the ferrite grains. Thus, H adsorption and H cluster formation at or near the grain boundaries are observed to affect the strength and failure modes of the grain boundaries.

Overall, the current study illustrates that H adsorption and accumulation near the interfacial regions in pearlitic steels has the potential to increase the strength of the ferrite–cementite interface as well as the ferrite–ferrite grain boundaries for some grain orientations. This observation is consistent with the trends observed in a previous study [21, 22], where nanoindentation experiments were used to demonstrate that the regions near such interfaces generally exhibited higher nano-hardness. Combining the current simulation results with additional experimental results and microstructural analyses, such as electron backscatter diffraction, would enable a more comprehensive understanding of the overall effects of H on the strength of pearlitic steels.

Conclusions

In the current study, molecular dynamics simulations were invoked to study H adsorption in pearlitic steels and its effect on the tensile strength of the ferrite–cementite phase boundaries and ferrite–ferrite grain boundaries. The thickness of the cementite phase and the orientation of the ferrite grain boundaries were observed to influence H adsorption and the strength of the corresponding phase and grain boundaries. A structure with thinner cementite adsorbed relatively more H atoms and exhibited increased interfacial strength. The extent of H adsorption and the strength of the Σ3 ferrite–ferrite grain boundaries were dependent on the orientation of the grain boundaries.

Acknowledgements The authors (Xiaoli Wang, Yonghao Zhao, Guang Cheng, Yang Zhang) acknowledge the support from the National Natural Science Foundation of China (51905026) and the Fundamental Research Funds for the Central Universities (buctrc201827). T.A. Venkatesh acknowledges support from the National Science Foundation (NSF-2119337).

References

1. R.A. Oriani, A mechanistic theory of hydrogen embrittlement of steels. Ber. Bunsenges. Phys. Chem. **76**, 848 (1972)
2. A.R. Troiano, The role of hydrogen and other interstitials in the mechanical behavior of metals. Metallogr. Microstruct. Anal. **5**, 557 (2016)
3. H.K. Birnbaum, P. Sofronis, Hydrogen-enhanced localized plasticity—a mechanism for hydrogen-related fracture. Mater. Sci. Eng. A **176**, 191 (1994)
4. P. Sofronis, H.K. Birnbaum, Mechanics of the hydrogen-dislocation-impurity interactions—I. Increasing shear modulus. J. Mech. Phys. Solids **43**, 49 (1995)
5. M. Nagumo, Hydrogen related failure of steels—a new aspect. Mater. Sci. Technol **20**, 940 (2004)
6. M. Nagumo, K. Takai, The predominant role of strain-induced vacancies in hydrogen embrittlement of steels: overview. Acta Mater. **165**, 722 (2019)
7. A. Ramasubramaniam, M. Itakura, E.A. Carter, Interatomic potentials for hydrogen in α–iron based on density functional theory. Phys. Rev. B **79**, 174101 (2009)
8. D. Xie, S. Li, M. Li, Z. Wang, P. Gumbsch, J. Sun, E. Ma, J. Li, Z. Shan, Hydrogenated vacancies lock dislocations in aluminium. Nat. Commun. **7**, 13341 (2016)
9. H.Y. Song, C.F. Li, S.F. Geng, M.R. An, M.X. Xiao, L. Wang, Atomistic simulations of effect of hydrogen atoms on mechanical behaviour of an α-Fe with symmetric tilt grain boundaries. Phys. Lett. A **382**, 2464 (2018)
10. J. Li, C. Lu, L. Pei, C. Zhang, R. Wang, K. Tieu, Effects of H segregation on shear-coupled motion of <110> grain boundaries in α-fe. Int. J. Hydrog. Energy **44**, 18616 (2019)
11. Y.-S. Chen, D. Haley, S.S.A. Gerstl, A.J. London, F. Sweeney, R.A. Wepf, W.M. Rainforth, P.A.J. Bagot, M.P. Moody, Direct observation of individual hydrogen atoms at trapping sites in a ferritic steel. Science **355**, 1196 (2017)
12. Y.-S. Chen, H. Lu, J. Liang, A. Rosenthal, H. Liu, G. Sneddon, I. McCarroll, Z. Zhao, W. Li, A. Guo, J.M. Cairney, Observation of hydrogen trapping at dislocations, grain boundaries, and precipitates. Science **367**, 171 (2020)
13. Y. Mishin, M. Asta, J. Li, Atomistic modeling of interfaces and their impact on microstructure and properties. Acta Mater. **58**, 1117 (2010)
14. J.A. Brown, Y. Mishin, Dissociation and faceting of asymmetrical tilt grain boundaries: molecular dynamics simulations of copper. Phys. Rev. B **76**, 134118 (2007)
15. A. Stukowski, Visualization and analysis of atomistic simulation data with OVITO–the open visualization tool. Modell. Simul. Mater. Sci. Eng. **18**, 015012 (2009)
16. A.P. Thompson, H.M. Aktulga, R. Berger, D.S. Bolintineanu, W.M. Brown, P.S. Crozier, P.J. in 't Veld, A. Kohlmeyer, S.G. Moore, T.D. Nguyen, R. Shan, M.J. Stevens, J. Tranchida, C. Trott, S.J. Plimpton, LAMMPS—a flexible simulation tool for particle-based materials modeling at the atomic, meso, and continuum scales. Comput. Phys. Commun. **271**, 108171 (2022)
17. L.S.I. Liyanage, S.-G. Kim, J. Houze, S. Kim, M.A. Tschopp, M.I. Baskes, M.F. Horstemeyer, Structural, elastic, and thermal properties of cementite (Fe_3C) calculated using a modified embedded atom method. Phys. Rev. B **89**, 094102 (2014)
18. S. Nouranian, M.A. Tschopp, S.R. Gwaltney, M.I. Baskes, M.F. Horstemeyer, An interatomic potential for saturated hydrocarbons based on the modified embedded-atom method. Phys. Chem. Chem. Phys. **16**, 6233 (2014)
19. M. Guziewski, S.P. Coleman, C.R. Weinberger, Atomistic investigation into the mechanical properties of the ferrite-cementite interface: the Bagaryatskii orientation. Acta Mater. **144**, 656 (2018)
20. P. Hirel, Atomsk: a tool for manipulating and converting atomic data files. Comput. Phys. Commun. **197**, 212 (2015)
21. G. Cheng, K.S. Choi, X. Hu, X. Sun, Determining individual phase properties in a multi-phase Q&P steel using multi-scale indentation tests. Mater. Sci. Eng. A **652**, 384 (2016)
22. G. Cheng, F. Zhang, A. Ruimi, D.P. Field, X. Sun, Quantifying the effects of tempering on individual phase properties of DP980 steel with nanoindentation. Mater. Sci. Eng. A **667**, 240 (2016)